

## Effects of high Z materials on $\pi_0$ reconstruction

L. Gilbert

July 18, 2013

MINER $\nu$ A is a low-energy neutrino scattering experiment on the NuMI beam-line at Fermilab. In this analysis, we studied the effect of small variations in the amount in non-instrumented high-Z materials in the EM calorimeter on pion reconstruction efficiency.

The EM calorimeter of MINER $\nu$ A is made of plastic scintillator bars. However, these bars do not make up the whole of the EM calorimeter; the bars are surrounded with support material. Each bar has a reflective coating of titanium dioxide and is held in place with a commercial epoxy. The interaction length of particles in the detector scales with the atomic number ( $Z$ ) of the material the particles pass through, as the likelihood of neutrino-nuclei interactions scales with number density of nuclei. Since the interaction length is an important part of event reconstruction, the atomic number (which also gives the number density of nuclei) should be simulated as accurately as possible.

Furthermore, interactions outside the fiducial volume will not be recorded. Such non-instrumented areas do not collect any data and any interactions that occur there are not included in the detector's digital output of the event. The detector simulation compensates for such events, but such compensation depends on the amount of material outside the fiducial volume. If the simulation has a substantially different amount of non-instrumented material than the real detector, this compensation will not be correct. The simulation will not be an accurate reconstruction of the detector.

When the detector was constructed, the precise amount of titanium dioxide

coating and epoxy used in the construction of EM calorimeter was not recorded. The amount of titanium dioxide used is known within a factor of two; the amount of grey epoxy to about 30%. The composition of the “grey epoxy” used to hold the bars in place is also a trade secret. Since both the composition of a given material and the amount of material used affect the interaction length, there is significant uncertainty in the interaction length of a pion in the EM calorimeter.

In this analysis, we simulated a variety of physically likely detector geometries to determine how our event reconstruction changes with the amount and composition of the “grey epoxy” and amount of titanium dioxide. From this, we can determine if the construction uncertainties are likely to affect our results.

We demonstrated that the composition of “grey epoxy” (% kaolin / hydrocarbon resin) used in the simulation does not substantially affect the reconstruction of Monte Carlo  $\pi_0$  events. If the amount of “grey epoxy” in the simulation is a factor of two higher or lower than the amount in the detector, there could be an effect of up to a  $\sim 5\%$  in reconstructed mass and energy. However, it is unlikely the simulation and the detector differ by enough to cause a statistically significant change in reconstructed pion mass and energy.

We also saw a  $\sim 5\%$  effect on both reconstructed mass and energy resolution by doubling the amount of reflective coating of the plastic scintillator bars in the simulation. Halving the amount of titanium dioxide coating showed no effect. As the uncertainty of the simulation estimate of the mass fraction of titanium dioxide could be up to a factor of two, the effects of the mass fraction of titanium dioxide on reconstruction should be studied further.

## Contents

<b>1</b>	<b>Introduction</b>	<b>2</b>
<b>2</b>	<b>Monte Carlo data and analysis</b>	<b>5</b>
2.1	Generation and reconstruction . . . . .	5
2.2	Variables analyzed . . . . .	5

<b>3</b>	<b>Uncertainties in Detector Composition and Structure</b>	<b>7</b>
3.1	Grey epoxy . . . . .	7
3.2	TiO <sub>2</sub> . . . . .	8
<b>4</b>	<b>High Z materials in grey epoxy</b>	<b>8</b>
4.1	Doubled amount of kaolin . . . . .	9
4.2	Halved amount of kaolin . . . . .	12
4.3	Density of kaolin . . . . .	15
<b>5</b>	<b>High Z titanium dioxide coating</b>	<b>21</b>
5.1	5xTiO <sub>2</sub> . . . . .	21
5.2	TiO <sub>2</sub> doubled . . . . .	29
5.3	TiO <sub>2</sub> halved . . . . .	35
5.4	Significance of results: halving, doubling, and reconstruction efficiency . . . . .	41
<b>6</b>	<b>Conclusions</b>	<b>42</b>

## 1 Introduction

MINER $\nu$ A is a neutrino scattering experiment focusing on improving the current limits on  $\Delta m_{13}$  and  $\theta_{13}$ , two of the unknown elements in the Pontecorvo-Maki-Nakagawa-Sakata lepton mixing matrix (MNS) matrix that determines neutrino oscillation, scattering, and mass. Additionally, neutrino-nucleus interactions have been little studied; MINER $\nu$ A will take detailed measurements of quasi-elastic scattering, coherent neutrino-nucleus scattering, and resonance-mediated processes.

MINER $\nu$ A uses scintillator plastic to detect the particles formed from a neutrino-nucleus interaction. Such particles are often mesons, which interact with the scintillator bars. When interactions occur, one or more photons are emitted. The scintillator bars are coated with titanium dioxide to create total internal reflection, and have a photomultiplier attached, translating the photon into a digital signal. Software then “reconstructs” the event, using the digital signals to determine where energy was deposited in the detector, and how much energy the interacting particle had.

This study focuses on the effects on digital event reconstruction of areas of the detector that do not record events, but in which mesons still interact – particularly, the effects of the construction materials around the scintillator bars. The bars are coated in highly reflective titanium dioxide (to prevent any light from escaping) and are glued together with a commercial epoxy.

The plastic scintillator used in MINER $\nu$ A is mostly hydrocarbons, while the epoxy is an alumina-silicate mixture. The reflective coating is made of  $\text{TiO}_2$  (79 amu/molecule). Both the alumina-silicate mixture and the titanium dioxide have a much higher atomic number ( $Z$ ) than the hydrocarbon-based scintillator plastic. The characteristic interaction length of a particle in a material scales with  $1/Z$ , so the amount of high  $Z$  material changes the interaction length of the detector as a whole. If the amount of high atomic number (high  $Z$ ) material in the detector differs from the amount used in the reconstruction process, the computer simulation will not accurately reconstruct the event.

The scintillator bars are not completely regular triangular prisms, as the corners are somewhat rounded (as shown in fig. 1). They were coated with roughly the same amount of  $\text{TiO}_2$  per bar, but the amount used during construction was not precisely measured. The official estimate of the amount of  $\text{TiO}_2$  coating used on the bars could differ from the actual amount by as much as a factor of five (up to a cm thickness).

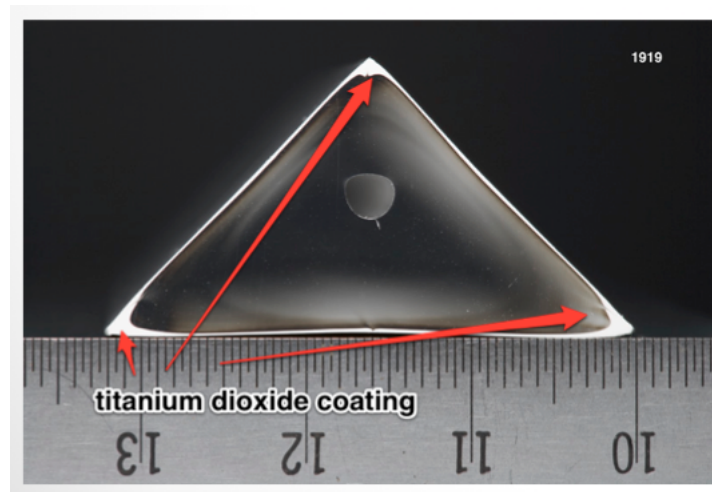


Figure 1: View of the cross-section of a scintillator bar from MINER $\nu$ A.

Collaborators involved in construction estimate the error on the official mass fraction of titanium dioxide is 20-50%, or 0.2 - 1 mm of thickness. In section 5, we determine if variations less than a factor of two in the amount of reflective coating affect our pion reconstruction efficiency, and if so, to what degree.

We also analyze the effects of the grey epoxy used to hold the bars together (section 4). It is commercially available, and as such, its manufacturers do not release the exact molecular mass or mass fraction of components. It is composed of kaolin, an alumina-silicate mineral, and a hydrocarbon-based resin. The analysis in section 4 discusses the current detector model and some refinements that would improve the model's accuracy.

Since  $\pi_0$  mesons are very common products of neutrino interactions, we simulate a “particle gun” of  $\pi_0$ s with known energies. The Monte Carlo events are described in more detail in 2.1.

We simulated a number of variations on the current geometry used in reconstruction (described in more detail in section 3) and analyzed the effects on reconstructed mass, reconstructed energy, energy resolution, and shower structure, comparing our modified reconstruction algorithm to an unmodified MINER $\nu$ A detector simulation.

## 2 Monte Carlo data and analysis

### 2.1 Generation and reconstruction

The analysis used 10000 event samples in which a  $\pi_0$  created at the interaction point (a “particle gun”). Energies of the pion ranged from 0 - 2 GeV. For all initial interactions,  $\phi$  (the polar angle in the transverse plane) = 0 and  $\theta$  (the angle between the particle track and the beam line) = 0. The Monte Carlo events were generated using software version v10r3p1.

We used the same Monte Carlo data with all detector simulations, to avoid statistic fluctuations. However, we used two reconstruction algorithms: Jose Palomino's MCPi0/AngleScan and Jeremy Wolcott's CCNuE/LowEnergyEM. There may be some difference in number of accepted events in variables associated with AngleScan (e.g. number of blobs) and those associated with CCNuE (e.g. GapScore1, GapScore2), as the cuts for accepted events in CCNuE and AngleScan are not the same.

For an event to be reconstructed, AngleScan requires two “blobs” (contiguous clusters of scintillator segments in which energy was deposited) and the total reconstructed mass of the event must be between  $100 \text{ MeV}/c^2$  and  $170 \text{ MeV}/c^2$ . CCNuE requires at least one track, no significant hadron calorimeter activity, and the prong intersect the tracker. CCNuE also rejects Michel electrons.

## 2.2 Variables analyzed

The output of each modified detector reconstructed was compared against the MinervaMaterials.xml reconstruction algorithm. The variables we compared were reconstructed mass, reconstructed energy and the energy resolution (reconstructed energy/Monte Carlo energy). We compared the percent difference between the two geometries for both mean and RMS values of all variables, as well as noting any odd events in the tails of the Lorentzian distributions.

Variables from AngleScan were calculated for every detector simulation with a unique geometry. Variables from CCNuE were used on all simulations that varied the mass fraction of titanium dioxide.

Additionally, we looked at the development and structure of the interaction shower. Once a neutrino interacts, two (or more) particles are produced, which interact further, until new particles no longer have sufficient momentum to create more particles. These chains of interactions cause multiple photons to be produced in the scintillator, and appear as cascading showers of interactions.

The CCNuE shower structure variables were:

- GapScore1: a quantitative value for the space between interaction points (that is, how “gappy” the shower is).

GapScore1 finds “pulse height peaks along shower axis, grows seeds, measures distance between edges (like a 1D blobber)”. It is “more likely to fail when confronted with a pile-up downstream” and is “more sensitive to small gaps” than GapScore2.

It organizes clusters by position along the shower axis, find the median energy deposition and median distance between clusters, considers the clusters in triples, and sums

the energy of clusters in each triplet. The gap score is calculated as follows:

$$d = \frac{(z_1 - z_2) + (z_3 - z_4)}{d_{median}} \quad (1)$$

$$\text{gap score} = \frac{d}{N_{triples}} \sum \frac{E_{median} - E_{triple}}{3E_{median}} \quad (2)$$

GapScore1 is zero in cases where the energy of a triplet is less than the median energy.

- GapScore2: a different quantitative value for the space between the interaction points. GapScore2 emphasizes the distance between successive low-pulse-height clusters. It is calculated by sorting clusters by position along Z axis, grouping clusters into bunches along shower axis and determining the mean cluster energy (total energy/number of bunches). The gap score is calculated with  $d$ , the distance between bunches,  $\Delta E_i$ , the difference between the energy of bunch  $i$  and the mean energy, and  $\Delta E_{i+1}$  the difference between the energy of bunch  $i+1$  and the mean energy.

$$d = \left( \frac{\min(z_{i+1}) - \max(z_i)}{\text{radiation length}} \right) \quad (3)$$

$$\Delta E_i = \left( 1 - \frac{2}{\pi} \arctan \left( \frac{|E_i - E_{mean}|}{E_{mean}} \right) \right) \quad (4)$$

$$\Delta E_{i+1} = \left( 1 - \frac{2}{\pi} \arctan \left( \frac{|E_{i+1} - E_{mean}|}{E_{mean}} \right) \right) \quad (5)$$

$$\text{gap score} = x \Delta E_i \Delta E_{i+1} \quad (6)$$

If there are less than two bunches in a given event, GapScore2 is zero.

- MedianPlaneShowerWidth: shows the transverse energy deposition profile and determines the median plane of scintillator in which interaction occurred. It is calculated by measuring median transverse length in strips in each plane (neighboring strips are merged together), and then taking the standard deviation of median transverse lengths.
- ShowerLengthEnergyScale: shows transverse energy deposition profile by measuring the distance between the first deposition of energy and the maximum energy deposition. It is calculated by finding the distance between the first deposition of energy and the Z position of the shower's maximum energy deposition, and dividing by the event energy.

Further information about the CCNuE shower structure variables can be found in Jeremy Wolcott's 2012 RochNu talk (Minerva Document 7183-v2).

AngleScan does not have detailed shower structure variables, but does calculate the number of blobs – that is, contiguous areas where energy was deposited – the event contained.

### 3 Uncertainties in Detector Composition and Structure

#### 3.1 Grey epoxy

The “grey epoxy” is made of two components: a low-Z resin (mostly hydrocarbons) and kaolin ( $\text{Al}_2\text{Si}_2\text{O}_5(\text{OH})_4$ ). The exact composition of the epoxy is a trade secret, so the precise ratio of kaolin and resin is unknown.

The amount used is relatively well known ( $\pm 30\%$ ) and fairly small.

#### 3.2 $\text{TiO}_2$

As discussed in the introduction, the scintillator bars are not perfectly regular — particularly, the edges are rounded and have a much thicker coating of  $\text{TiO}_2$  than the rest of the bar. The coating thickness can vary by up to 5 mm.

There is little difference between bars; the total amount of  $\text{TiO}_2$  (as determined from photographs) is fairly similar for all bars (as shown in fig. 2).

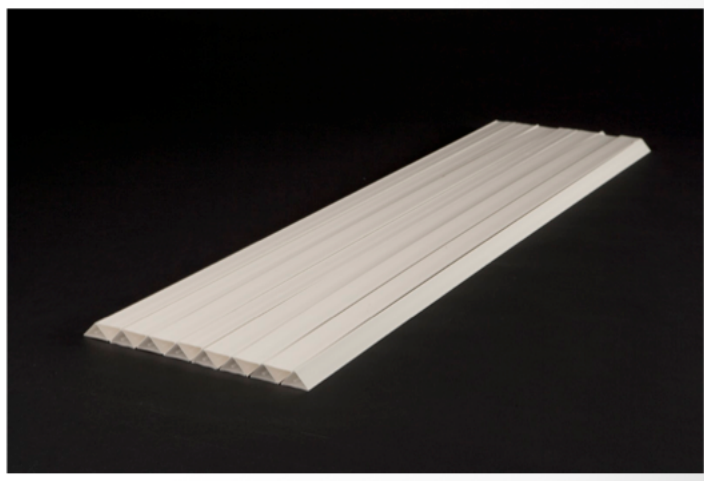


Figure 2: 15 scintillator bars with reflective coating

Our estimates from photographs suggest that the amount of  $\text{TiO}_2$  the detector simulation



may be off by as much a factor of two. Collaboration members involved in the construction of the scintillator bars think that the detector simulation is likely within 40% of the true amount of  $\text{TiO}_2$  used.

## **4 High Z materials in grey epoxy**

As mentioned in section 3.1, the grey epoxy consists of two parts: a hydrocarbon-based resin and kaolin. We simulated a variation in the ratio of resin and kaolin, changing the effective density of the epoxy. The volume of grey epoxy is unchanged, but the mass of grey epoxy changed as the ratio of components changed.

### **4.1 Doubled amount of kaolin**

We doubled the amount of kaolin to 30% by weight of the epoxy (70% low Z resin). Comparison plots for reconstruction with this geometry and 15% epoxy are shown in figs. 3 - 6. The results are summarized in table 1.

This shows a shift in reconstructed mass. However, collaborators involved in construction of the grey epoxy believe this is an extreme overestimate — the epoxy was likely much less than 30% kaolin.

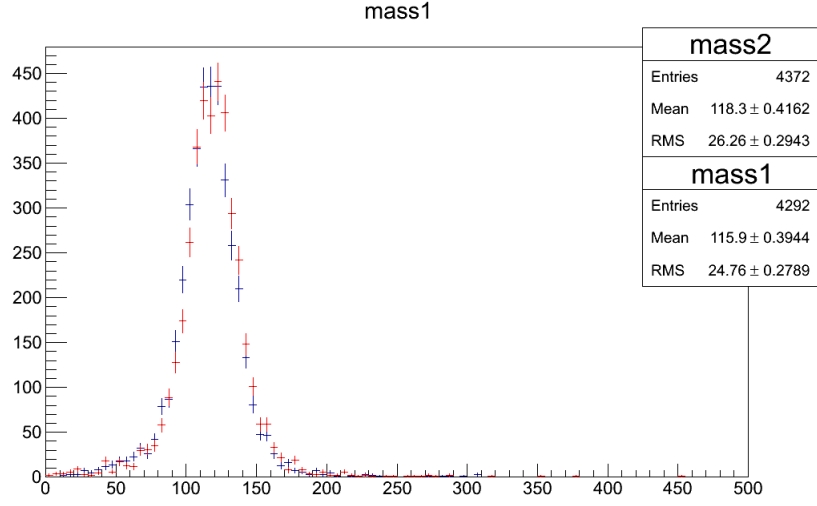


Figure 3: Reconstructed  $\pi_0$  mass (in  $\text{MeV}/c^2$ ) vs. number of events. mass1 (in blue) depicts the reconstructed mass with the original simulation; mass2 (in red) depicts the reconstructed mass from the simulation with 30% kaolin, 70% resin.

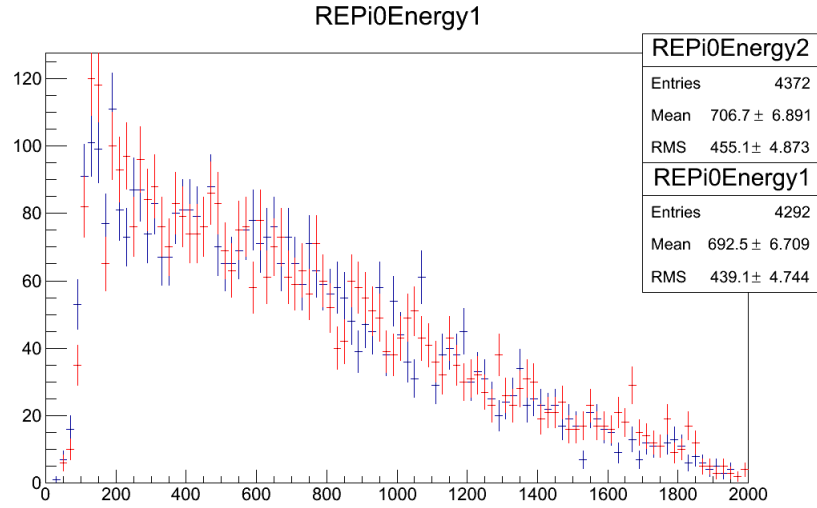


Figure 4: Reconstructed  $\pi_0$  energy (in MeV) vs. number of events. REPi0Energy1 (in blue) depicts the reconstructed mass with the original simulation; REPi0Energy2 (in red) depicts the reconstructed energy from the simulation with 30% kaolin, 70% resin.

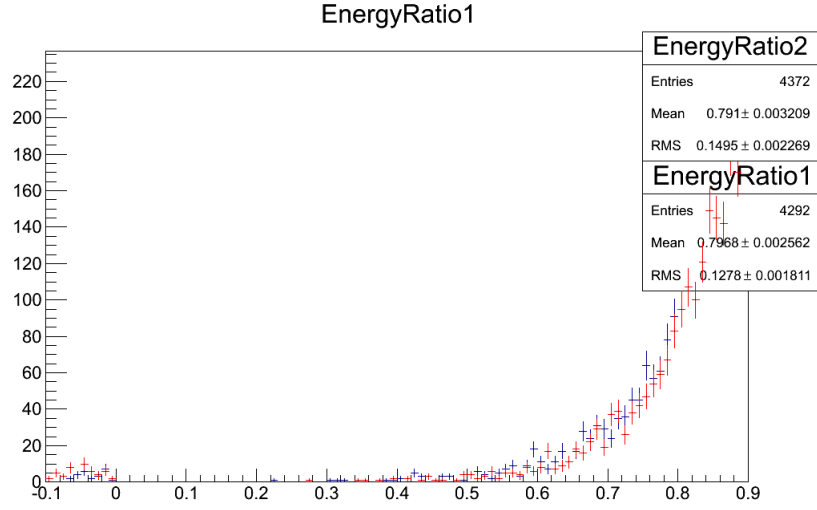


Figure 5: Ratio of reconstructed  $\pi_0$  energy / Monte Carlo energy vs. number of events. EnergyRatio1 (in blue) depicts the reconstructed mass with the original simulation; EnergyRatio2 (in red) depicts the reconstructed mass from the simulation with 30% kaolin, 70% resin.

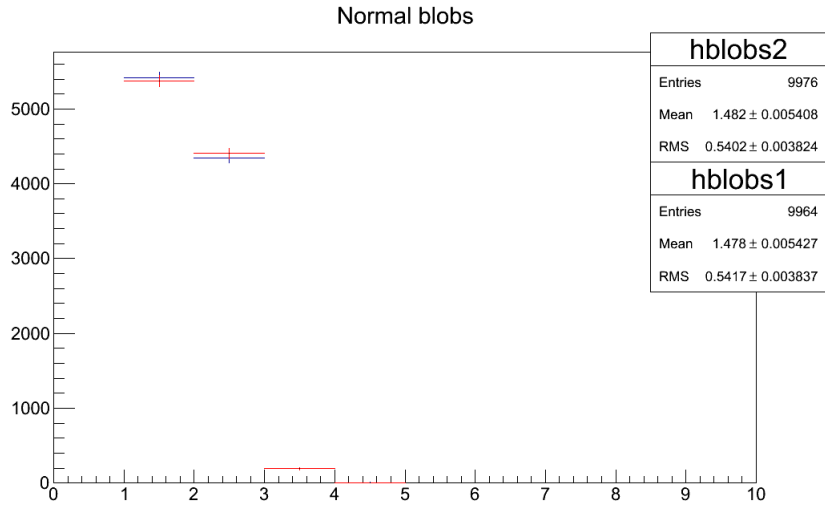


Figure 6: Number of AngleScan “blobs” vs. number of events. hblobs1 (in blue) depicts the reconstructed mass with the original simulation; hblobs2 (in red) depicts the reconstructed mass from the simulation with 30% kaolin, 70% resin.

Variable	15% kaolin, 85% resin	30% kaolin, 70% resin	% difference
Mass (mean, MeV/c <sup>2</sup> )	115.9	118.3	2.04%
Mass (rms, MeV/c <sup>2</sup> )	24.76	26.26	5.88%
Energy (mean, MeV)	692.5	706.7	2.02%
Energy (rms, MeV)	439.1	455.1	3.57%
EnergyRatio (mean)	0.7968	0.791	0.73%
EnergyRatio (rms)	0.1278	0.1495	15.65%
Number of blobs (mean)	1.478	1.482	0.27%
Number of blobs (rms)	0.5417	0.5402	0.277%

Table 1: Summary of variables and percent differences between simulation with 30% kaolin, 70% resin and simulation with original mass fractions

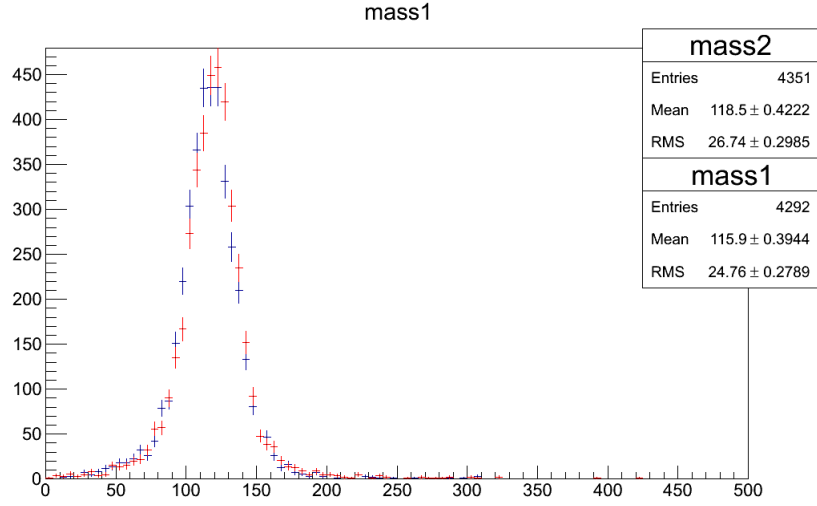


Figure 7: Reconstructed  $\pi_0$  mass (in  $\text{MeV}/c^2$ ) vs. number of events. mass1 (in blue) depicts the reconstructed mass with the original simulation; mass2 (in red) depicts the reconstructed mass from the simulation with 7.5% kaolin, 92.5% resin.

## 4.2 Halved amount of kaolin

We halved the amount of kaolin to 7.5% of the epoxy (92.5% resin). Comparison plots for reconstruction with this geometry and 15% kaolin, 85% resin are shown in figs. 7 - 10. The results are summarized in table 2.

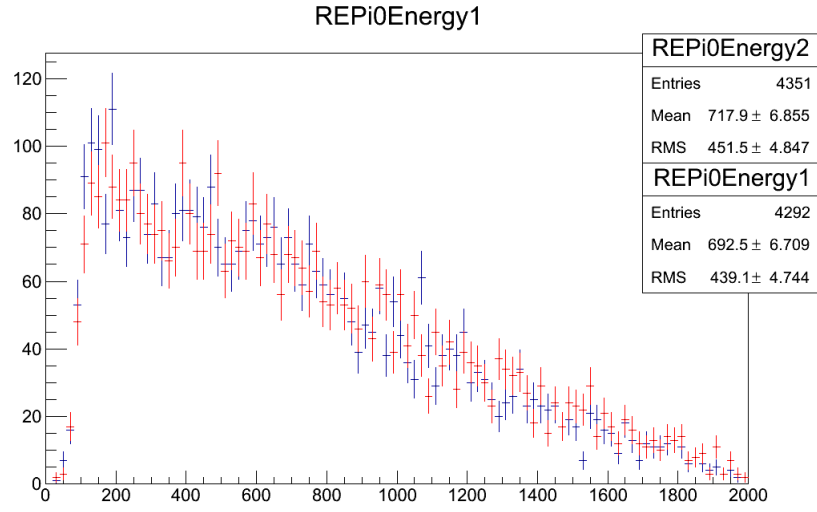


Figure 8: Reconstructed  $\pi_0$  energy (in MeV) vs. number of events. REPi0Energy1 (in blue) depicts the reconstructed mass with the original simulation; mass2 (in red) depicts the reconstructed energy from the simulation with 7.5% kaolin, 92.5%.

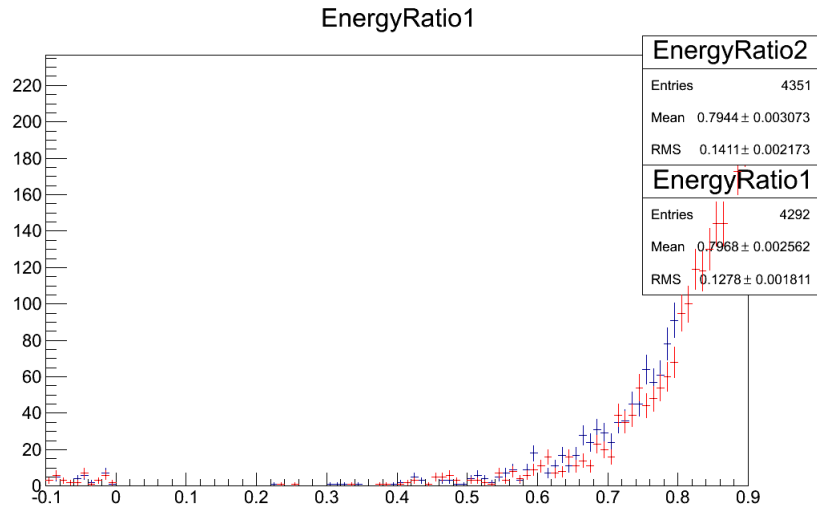


Figure 9: Ratio of reconstructed  $\pi_0$  energy / Monte Carlo energy vs. number of events. EnergyRatio1 (in blue) depicts the reconstructed mass with the original simulation; EnergyRatio2 (in red) depicts the reconstructed mass from the simulation with 7.5% kaolin, 92.5% resin.

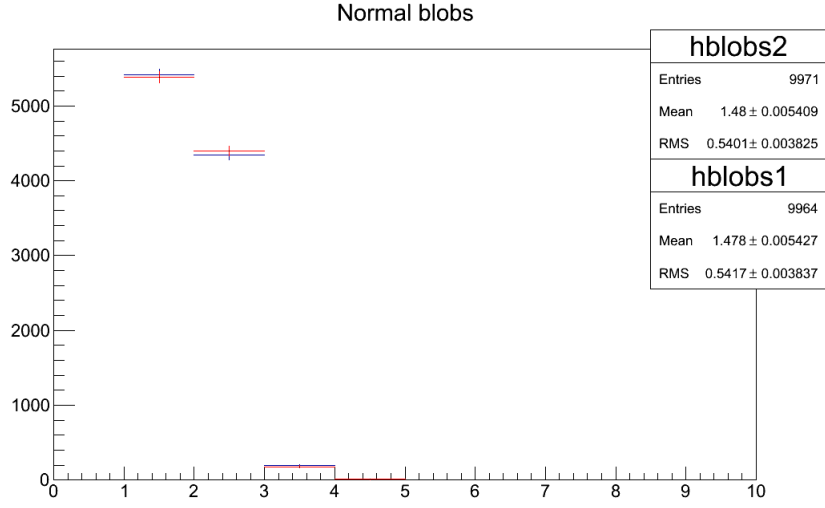


Figure 10: Number of AngleScan “blobs” vs. number of events. hblobs1 (in blue) depicts the reconstructed mass with the original simulation; hblobs2 (in red) depicts the reconstructed mass from the simulation with 7.5% kaolin, 92.5% resin.

Variable	15% kaolin, 85% resin	7.5% kaolin, 92.5% resin	% difference
Mass (mean, $\text{MeV}/c^2$ )	115.9	118.5	2.21%
Mass (rms, $\text{MeV}/c^2$ )	24.76	26.74	7.68%
Energy (mean, MeV)	692.5	717.9	3.60%
Energy (rms, MeV)	439.1	451.5	2.78%
EnergyRatio (mean)	0.7968	0.7944	0.31%
EnergyRatio (rms)	0.1278	0.1411	9.89%
Number of blobs (mean)	1.478	1.48	0.13%
Number of blobs (rms)	0.5417	0.5401	0.29%

Table 2: Summary of variables and percent differences between simulation with 7.5% kaolin, 92.5% resin and simulation with original mass fractions

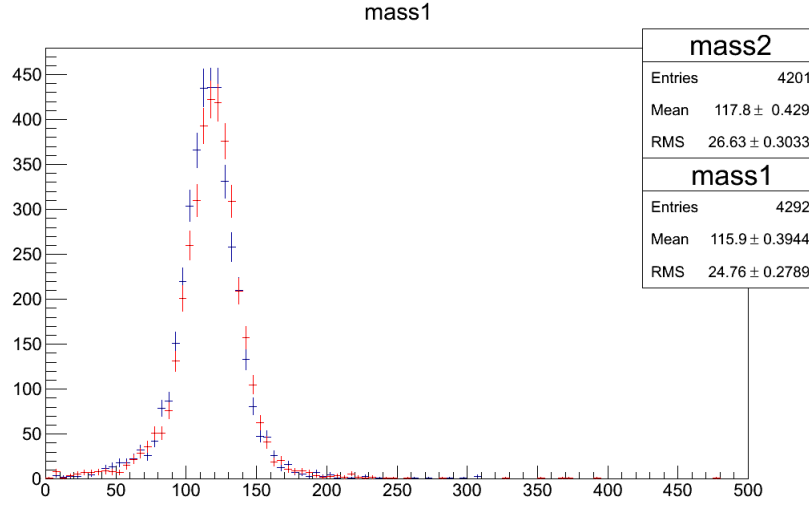


Figure 11: Reconstructed  $\pi_0$  mass (in  $\text{MeV}/c^2$ ) vs. number of events. mass1 (in blue) depicts the reconstructed mass with the higher density; mass2 (in red) depicts the reconstructed mass with the MSDS density value.

### 4.3 Density of kaolin

The MSDS for the epoxy<sup>1</sup> indicates the “kaolin” in the epoxy is not pure kaolin. The technical specifications for the epoxy list a significantly lower density for kaolin mixture ( $1.33 \text{ g/cm}^3$ ) than pure kaolin, but our detector specifications use the density of pure kaolin ( $2.6 \text{ g/cm}^3$ ). The MSDS also suggests that the mass ratio is closer to 20% kaolin, 80% resin than our original estimate of 15% kaolin, 85% resin.

We plotted the variables described in sec. 2.2 with the modified density for kaolin in figs. 11 - 18. Table 3 summarizes the changes in mean and rms values.

Only the root-mean-squared (RMS) reconstructed mass showed a  $>5\%$  effect, and the mean reconstructed mass did not show a particularly significant change. Furthermore, we see no significant differences in the shape of the plots. While it does appear that the density currently listed in MinervaMaterials is wrong, the mistake should not affect our reconstruction.

<sup>1</sup>[http://multimedia.3m.com/mws/mediawebserver?mwsId=SSSSSuUn\\_zu8l00x4Yt94x\\_Gnv70k17zHvu9lxtD7SSSSSS--](http://multimedia.3m.com/mws/mediawebserver?mwsId=SSSSSuUn_zu8l00x4Yt94x_Gnv70k17zHvu9lxtD7SSSSSS--)



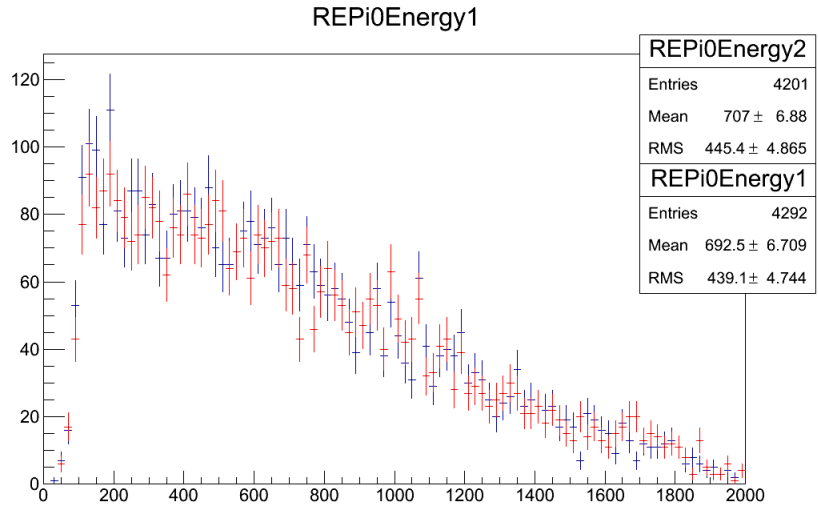


Figure 12: Reconstructed  $\pi_0$  energy (in MeV) vs. number of events. REPi0Energy1 depicts the reconstruction with the higher density (that of pure kaolin), while REPi0Energy2 depicts the reconstruction with the MSDS density value.

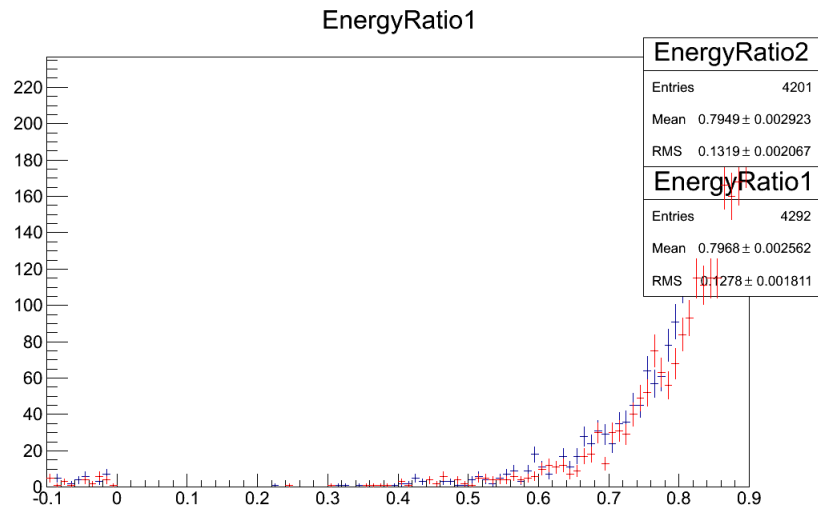


Figure 13: Ratio of reconstructed  $\pi_0$  energy / Monte Carlo energy vs. number of events. EnergyRatio1 depicts the reconstruction with the higher density (that of pure kaolin), while EnergyRatio2 depicts the reconstruction with the MSDS density value.

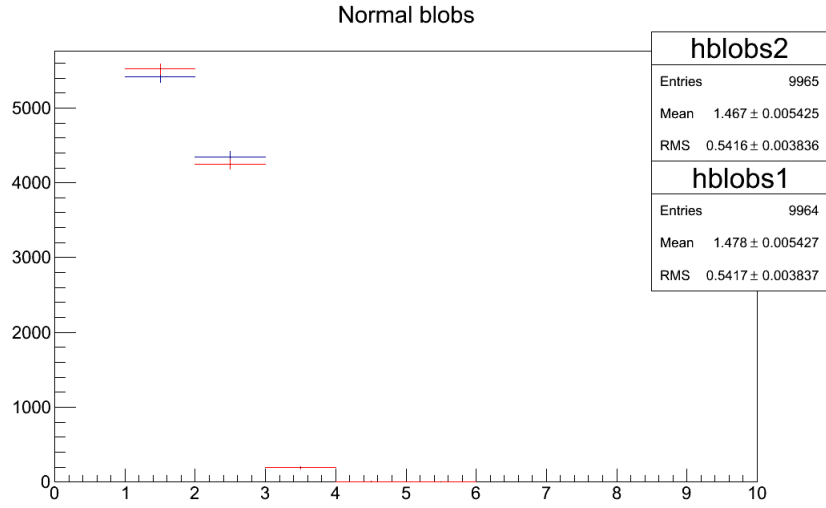


Figure 14: Number of AngleScan “blobs” vs. number of events. As above, hblobs1 (blue) depicts the original geometry; hblobs2 (red) depicts the MSDS density value.

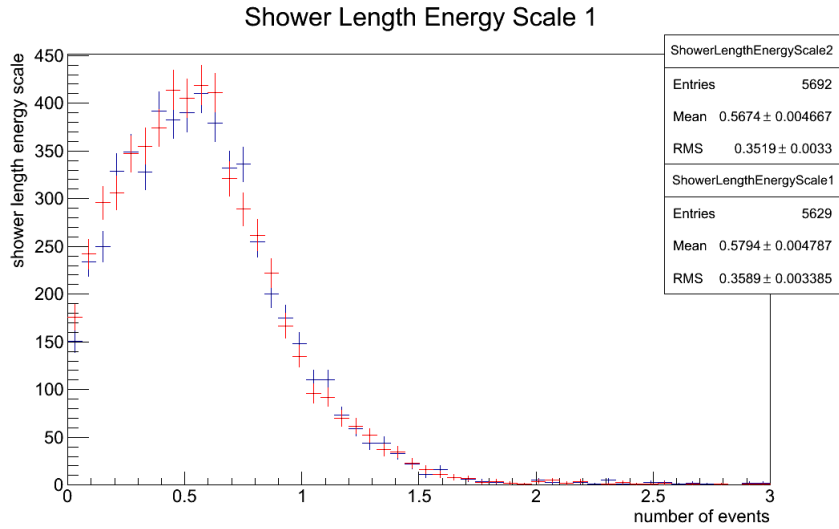


Figure 15: CCNuE Shower length energy scale (measured in mm/eV), as described in section 2.2. The plot in blue (ShowerLengthEnergyScale1) is the original; the plot in red (ShowerLengthEnergyScale2) shows the modified density.

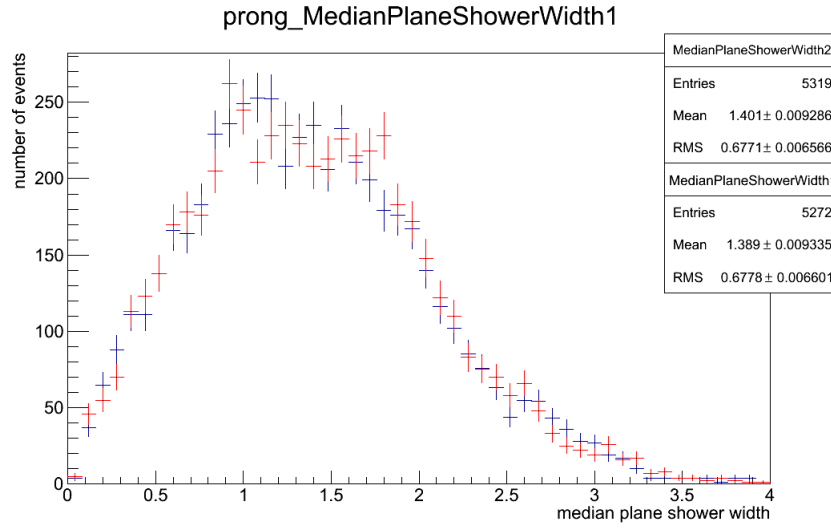


Figure 16: Median plane shower width (strip number) vs. number of events, as described in section 2.2. The plot in blue (MedianPlaneShowerWidth1) is the original with pure kaolin; the plot in red (ShowerLengthEnergyScale2) shows the density of the kaolin mixture indicated in the MSDS.

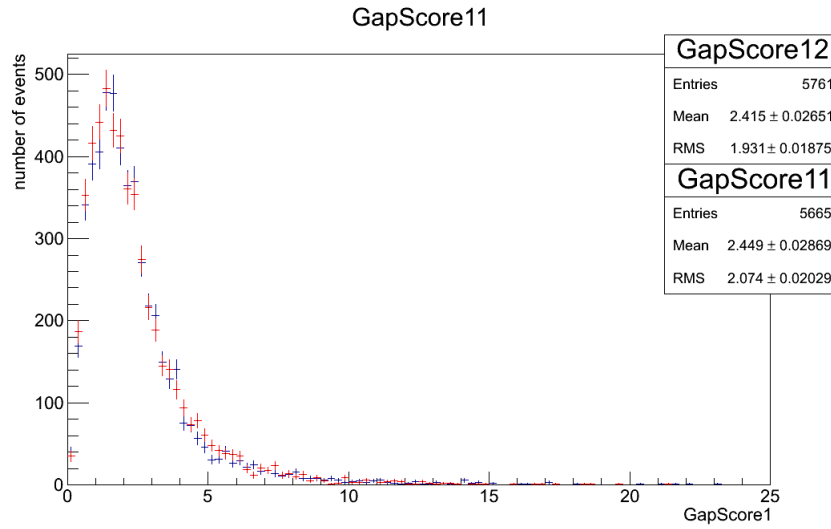


Figure 17: GapScore1 (unitless), the calculation of which is described in section 2.2. The blue is GapScore11 and shows the initial reconstruction; the red is GapScore21 and shows the reconstruction based on the corrected density.

Variable	2.6 g/cm <sup>3</sup>	1.33 g/cm <sup>3</sup>	% difference
ShowerLengthEnergyScale (mean, mm/eV)	0.5794	0.5674	2.09%
ShowerLengthEnergyScale (rms, mm/eV)	0.3589	0.3519	1.96%
MedianPlaneShowerWidth (mean)	1.389	1.401	0.86%
MedianPlaneShowerWidth (rms)	0.668	0.6671	0.13%
GapScore2 (mean)	0.4806	0.4732	1.55%
GapScore2 (rms)	0.3682	0.3806	3.31%
GapScore1 (mean)	2.449	2.415	3.31%
GapScore1 (rms)	2.074	2.931	7.14%
Mass (mean, MeV/c <sup>2</sup> )	115.9	117.8	1.62%
Mass (rms, MeV/c <sup>2</sup> )	24.76	26.63	7.27%
Energy (mean, MeV)	692.5	707	2.07%
Energy (rms, MeV)	439.1	445.4	1.47%
EnergyRatio (mean)	0.7968	0.7949	0.23%
EnergyRatio (rms)	0.1278	0.1319	3.15%
Number of blobs (mean)	1.478	1.467	0.74%
Number of blobs (rms)	0.5417	0.5416	0.01%

Table 3: Summary of variables and percent differences between simulation with corrected kaolin density and simulation with original density

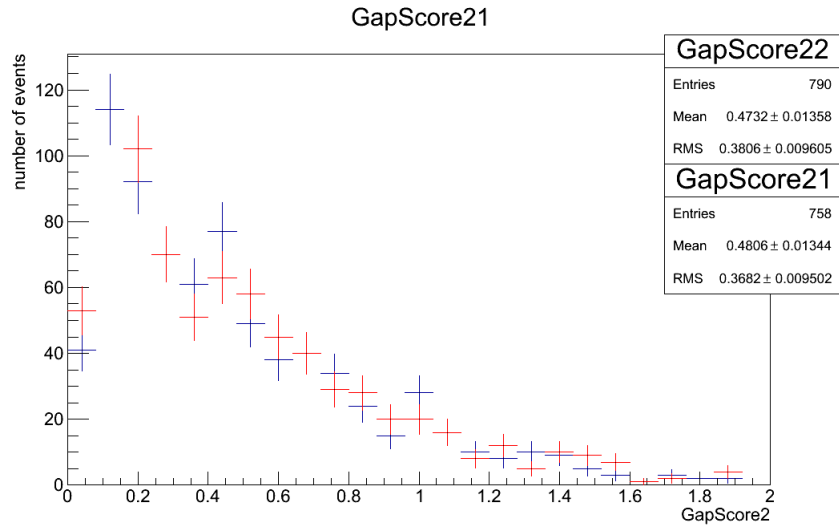


Figure 18: GapScore2 (unitless), the calculation of which is described in section 2.2. The blue is GapScore21 and shows the initial reconstruction; the red is GapScore22 and shows the reconstruction based on the corrected density.

Even so, it is an extremely minor fix and make our reconstruction more like the real detector. The official detector simulation (MinervaMaterials.xml) should be changed to match the MSDS density and mass fraction.

## 5 High Z titanium dioxide coating

We changed the amount of reflective coating in MinervaMaterials.xml by changing the mass fraction for the plastic scintillator bars. By default, the scintillator bars were 15%  $\text{TiO}_2$  by mass; 85% plastic scintillator. The volume of the bars was fixed, so by changing the mass fraction, we effectively reduced the total mass of scintillator and increased the total mass of  $\text{TiO}_2$ . Since  $\text{TiO}_2$  is denser than scintillator, this also increased the total mass of the bars.

### 5.1 5x $\text{TiO}_2$

Before simulating more likely geometries, we used a reconstruction with far more titanium dioxide (75% by mass) than plastic scintillator (25% by mass). This should have significantly reduced the interaction length and impaired our reconstruction; if it did not, the simulation and reconstruction were flawed. Before we could conclude that a given geometry change was insignificant, we needed to demonstrate it was possible to make a significant change.

Variables are plotted in figs. 19 - 26, and a summary of the variables is included in table 4. As expected, the atomic number used of the material used for the electromagnetic calorimeter does matter. It was a bit surprising that the reconstructed mass did not change, but the reconstructed energy and energy ratio changed quite a bit. This demonstrates that it is *possible* that the reflective coating could affect results. It does not prove that the amount of reflective coating *definitely* changes the reconstruction, as this geometry is highly exaggerated.

Variable	15% TiO <sub>2</sub>	75% TiO <sub>2</sub>	% difference
Mass (mean, MeV/c <sup>2</sup> )	115.9	105.6	9.30%
Mass (rms, MeV/c <sup>2</sup> )	24.76	23.91	3.49%
Energy (mean, MeV)	692.5	633.1	8.96%
Energy (rms, MeV)	439.1	409.5	6.97%
EnergyRatio (mean)	0.7968	0.7722	3.13%
EnergyRatio (rms)	0.1278	0.1057	18.92%
Number of blobs (mean)	1.478	1.469	0.61%
Number of blobs (rms)	0.5417	0.5486	1.26%
ShowerLengthEnergyScale (mean, mm/eV)	0.5794	0.5815	0.361%
ShowerLengthEnergyScale (rms, mm/eV)	0.3589	0.3787	8.19%
MedianPlaneShowerWidth (mean)	1.389	1.38	0.650%
MedianPlaneShowerWidth (rms)	0.677	0.6328	6.86%
GapScore2 (mean)	0.4806	0.4814	0.16%
GapScore2 (rms)	0.3682	0.3552	3.59%
GapScore1 (mean)	2.449	2.217	9.94%
GapScore1 (rms)	2.074	1.992	4.03%

Table 4: Comparison of variables for scintillator composed of 75% TiO<sub>2</sub> by volume (five times the original amount) and 15% TiO<sub>2</sub> by volume (original detector simulation)

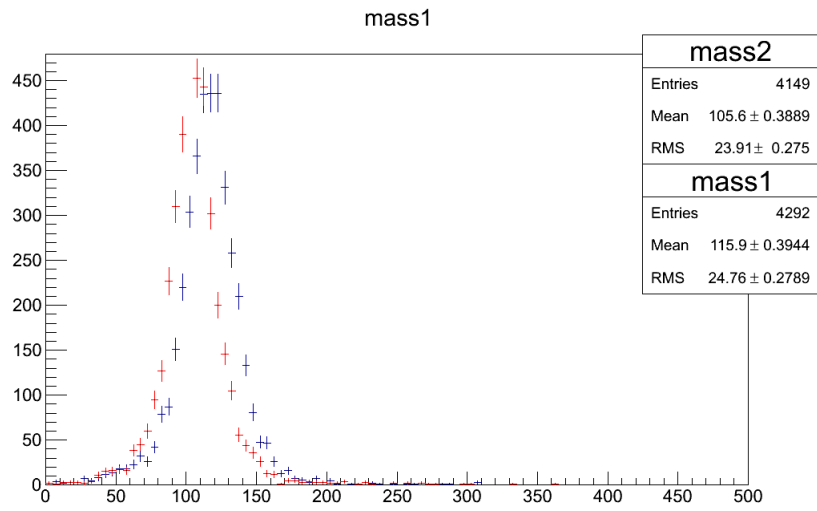


Figure 19: Reconstructed  $\pi_0$  mass (in  $\text{MeV}/c^2$ ) vs. number of events. mass1 (in blue) depicts the reconstructed mass with the original simulation; mass2 (in red) depicts the reconstructed mass from the simulation if we simulate the scintillator section of the detector as 75%  $\text{TiO}_2$  by mass, and only 25% plastic scintillator.



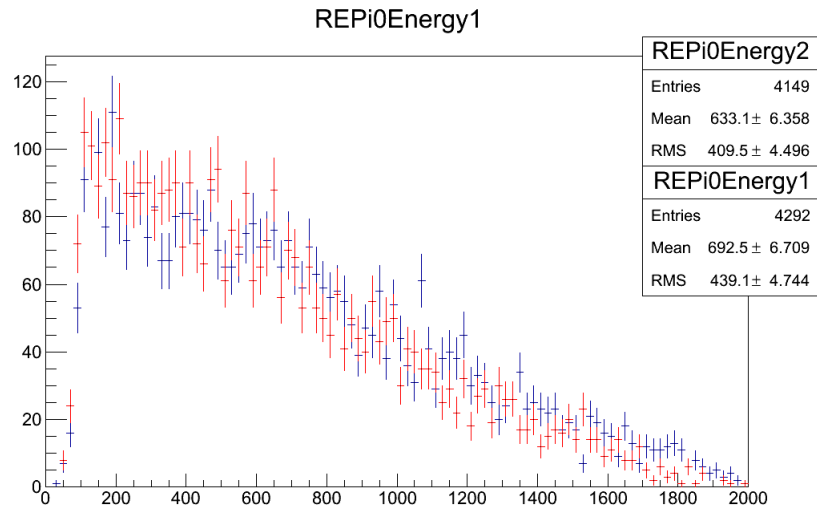


Figure 20: Reconstructed  $\pi_0$  energy (in MeV) vs. number of events. REPi0Energy1 (in blue) depicts the reconstructed mass with the original simulation; REPi0Energy2 (in red) depicts the reconstructed mass from the simulation if we simulate the scintillator section of the detector as 75%  $\text{TiO}_2$  by mass, and only 25% plastic scintillator.

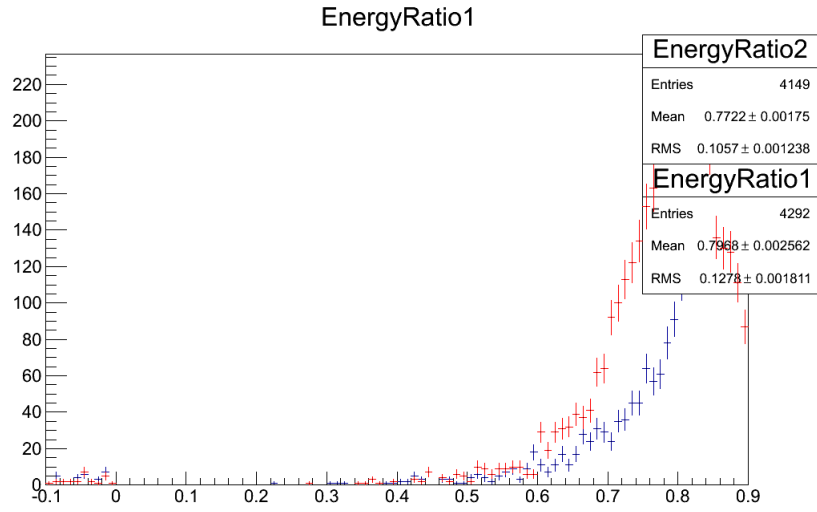


Figure 21: Reconstructed  $\pi_0$  energy / Monte Carlo energy vs. number of events. EnergyRatio1 (in blue) depicts the reconstructed mass with the original simulation; EnergyRatio2 (in red) depicts the reconstructed mass from the simulation if we simulate the scintillator section of the detector as 75%  $\text{TiO}_2$  by mass, and only 25% plastic scintillator.

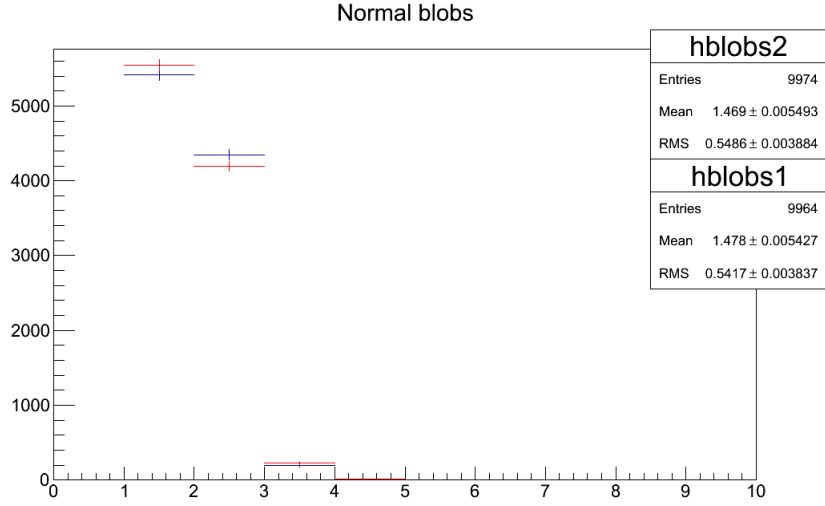


Figure 22: Number of “AngleScan” blobs vs. number of events. nblobs1 (in blue) depicts the reconstructed mass with the original simulation; nblobs2 (in red) depicts the reconstructed mass from the simulation if we simulate the scintillator section of the detector as 75%  $\text{TiO}_2$  by mass, and only 25% plastic scintillator.

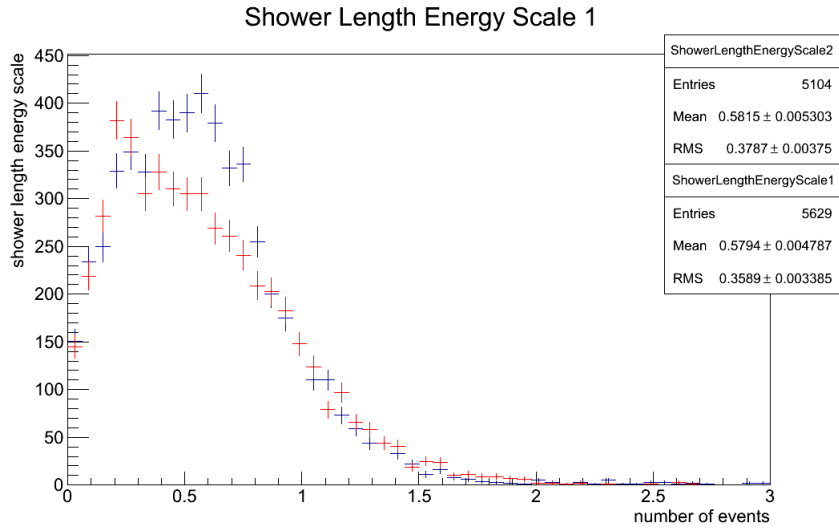


Figure 23: Shower length energy scale or energy deposition profile (mm/eV). Algorithm described in section 2.2. ShowerLengthEnergyScale1 (blue) depicts 15%  $\text{TiO}_2$  by mass; ShowerLengthEnergyScale2 (red) depicts 75%  $\text{TiO}_2$  by mass.

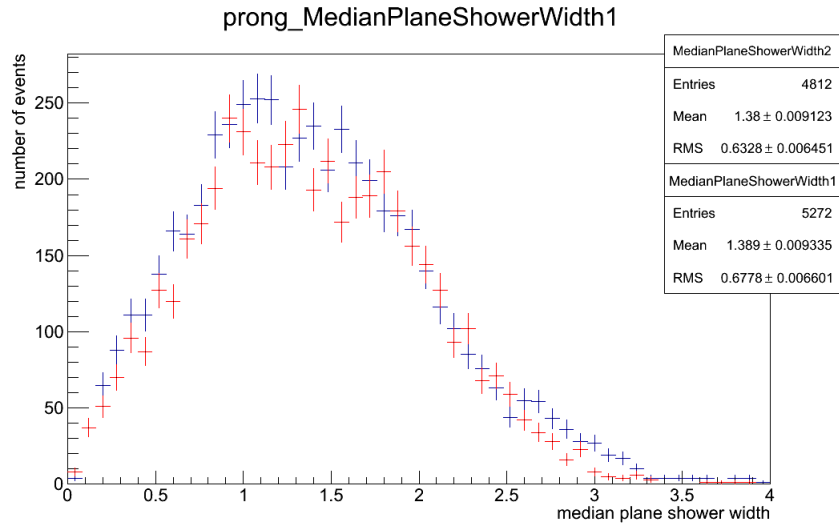


Figure 24: Median plane of deposition (strip number), which shows the shower width. Details of calculation are described in 2.2. MedianPlaneShowerWidth1 depicts 15%  $\text{TiO}_2$  by mass; MedianPlaneShowerWidth2 depicts 75%  $\text{TiO}_2$  by mass.

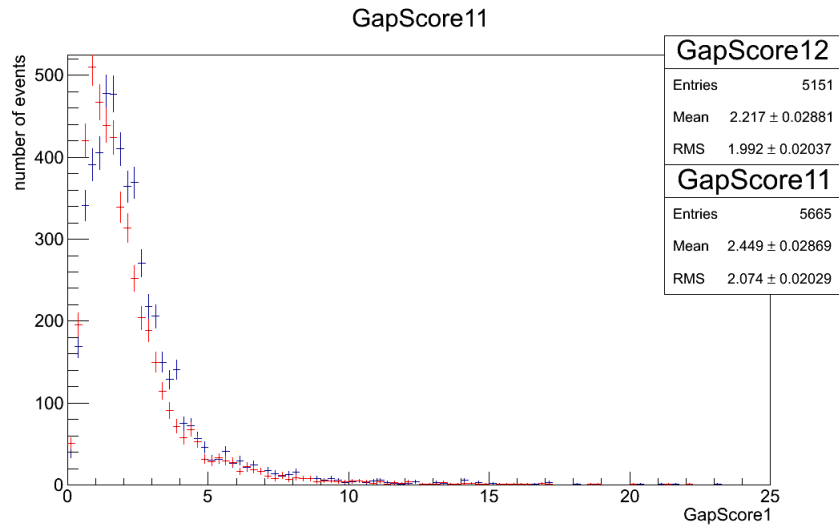


Figure 25: GapScore1, which indicates how spread apart the energy deposition of the shower was. The calculation of GapScore1 is described in sec. 2.2. GapScore11 depicts 15%  $\text{TiO}_2$ ; GapScore21 depicts a scintillator region of 75%  $\text{TiO}_2$ .

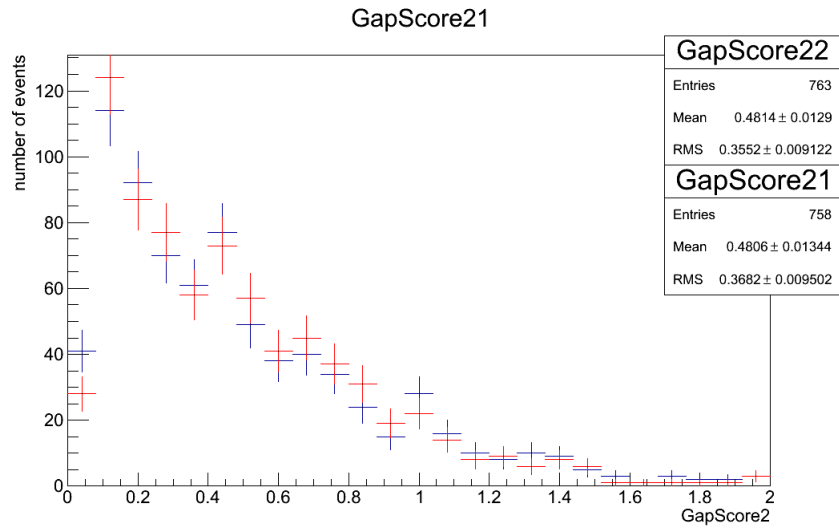


Figure 26: GapScore2, which indicates distance between low-peak-height clusters. The calculation of GapScore2 is described in sec. 2.2. GapScore21 depicts 15%  $\text{TiO}_2$ ; GapScore22 depicts a scintillator region of 75%  $\text{TiO}_2$ .

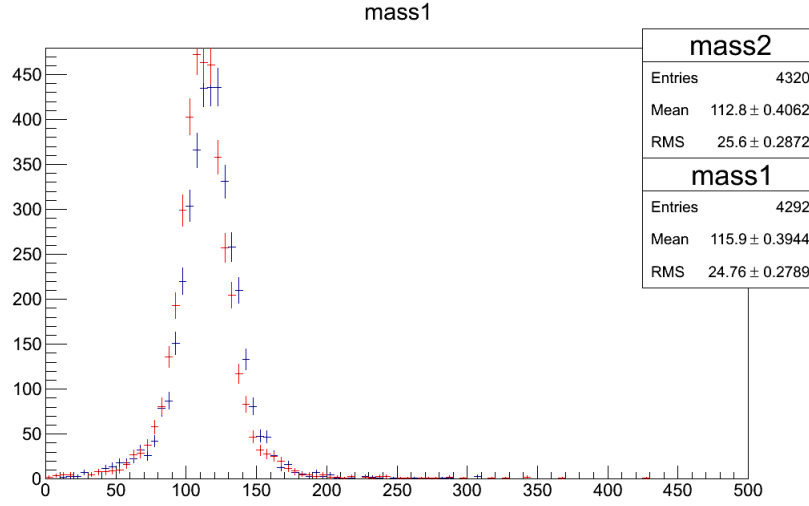


Figure 27: Reconstructed mass of  $\pi_0$  particles (in  $\text{MeV}/c^2$ ) vs. number of events. mass1 (blue) depicts 15%  $\text{TiO}_2$  bars by mass; mass2 (red) depicts 30%  $\text{TiO}_2$  by mass.

## 5.2 $\text{TiO}_2$ doubled

In this geometry, the scintillator bars were 70% plastic scintillator by mass, 30%  $\text{TiO}_2$ . Based on our photos of the construction, we believe this is the absolute upper limit of  $\text{TiO}_2$  used. According to collaborators who supervised construction, the error in amount of  $\text{TiO}_2$  is more likely to be 30%-40%, not 200%.

We plotted the variables described in sec. 2.2 with the 75% titanium dioxide, 25% plastic scintillator by mass bars in figs. 27 - 34.

We summarize the differences between the unmodified geometry and a geometry with doubled titanium dioxide content in table 5.2.

This is a significant effect. The reconstructed mass shifts by 3% (around 3 MeV), and the RMS energy ratio shows a change of more than 10%. As the reconstructed mass is one of the most important variables for particle identification, this could impact our results. Furthermore, we see a significant change in shape in the energy ratio plot (fig. 29).

If there is a even a remote possibility that this much titanium dioxide was used, further investigation is called for.

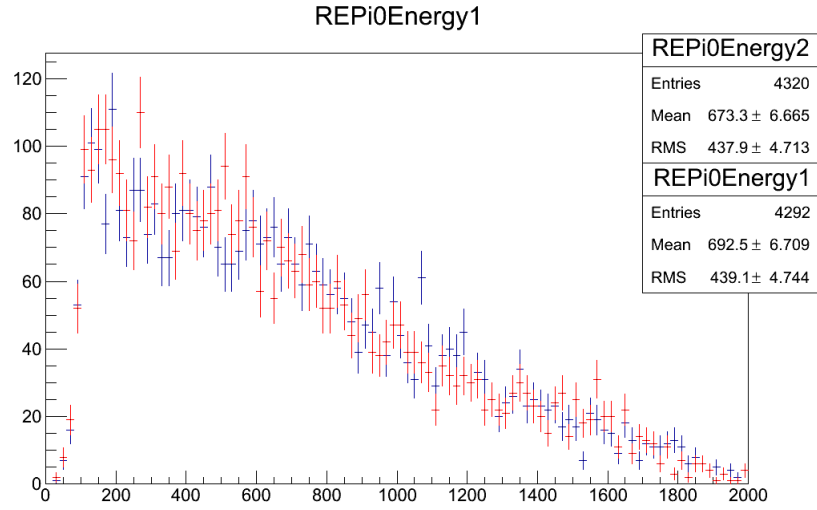


Figure 28: Reconstructed energy of  $\pi_0$  particles (in MeV) vs. number of events. energy1 (blue) depicts 15%  $\text{TiO}_2$  bars by mass; energy2 (red) depicts 30%  $\text{TiO}_2$  by mass.

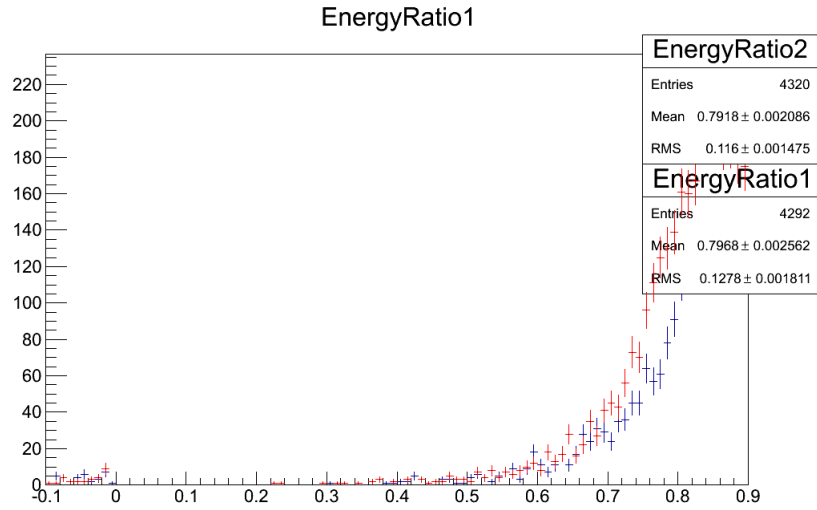


Figure 29: Ratio of reconstructed energy / Monte Carlo energy vs. number of events. Energy-Ratio1 (blue) depicts 15%  $\text{TiO}_2$  bars by mass; EnergyRatio2 (red) depicts 30%  $\text{TiO}_2$  by mass.

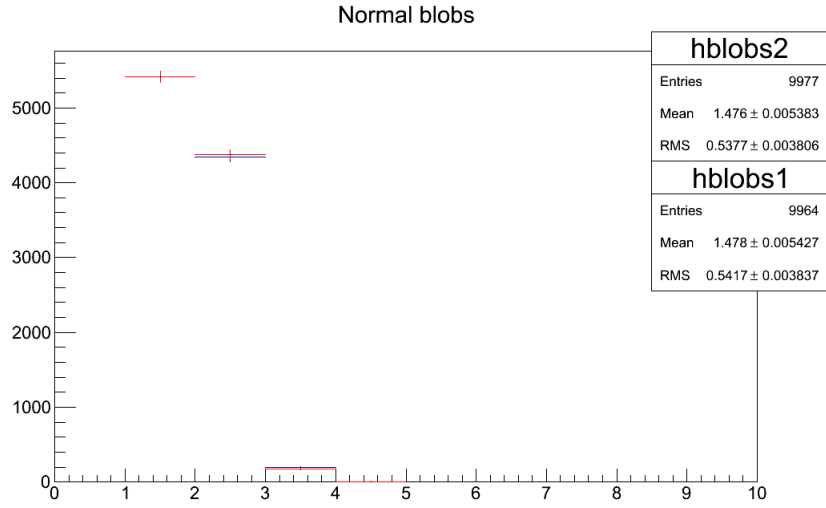


Figure 30: Number of AngleScan blobs vs. number of events. nblobs1 (blue) depicts 15%  $\text{TiO}_2$  bars by mass; nblobs2 (red) depicts 30%  $\text{TiO}_2$  by mass.

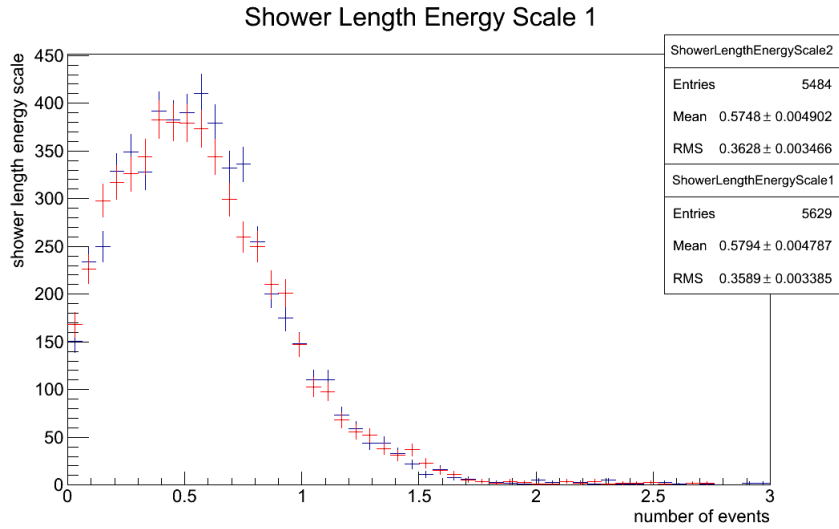


Figure 31: Shower length energy scale (mm/eV) or energy deposition profile. Algorithm described in section 2.2. ShowerLengthEnergyScale1 (blue) depicts 15%  $\text{TiO}_2$  by mass; ShowerLengthEnergyScale2 (red) depicts 30%  $\text{TiO}_2$  by mass.



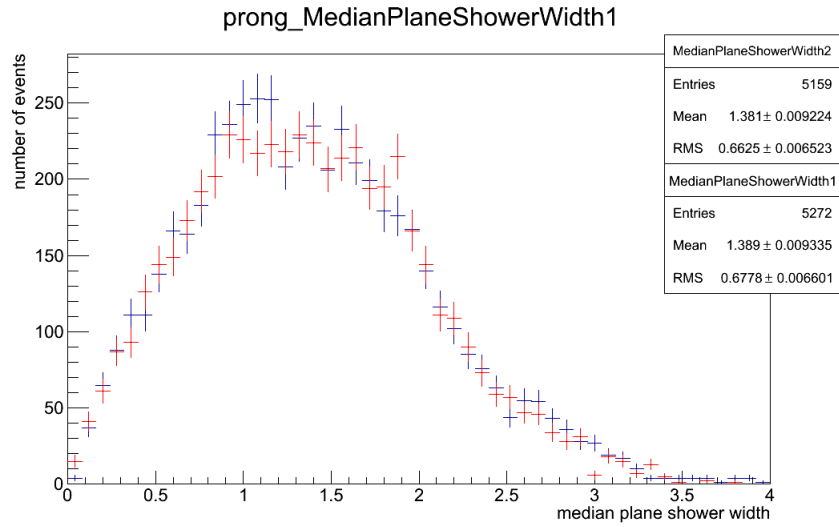


Figure 32: Median plane of deposition (strip number), which shows the shower width. Details of calculation are described in 2.2. MedianPlaneShowerWidth1 depicts 15%  $\text{TiO}_2$  by mass; MedianPlaneShowerWidth2 depicts 30%  $\text{TiO}_2$  by mass.

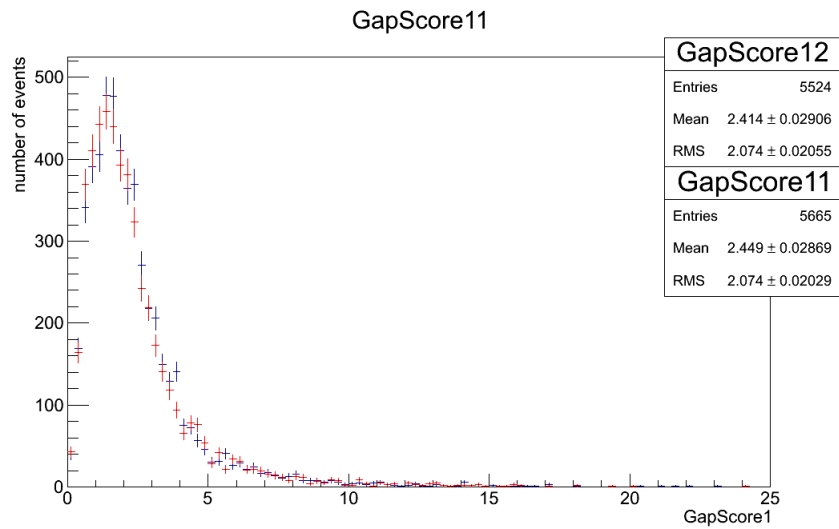


Figure 33: GapScore1, which indicates how spread apart the energy deposition of the shower was. The calculation of GapScore1 is described in sec. 2.2. GapScore11 depicts 15%  $\text{TiO}_2$ ; GapScore21 depicts a coating of 30%  $\text{TiO}_2$ .

Variable	15% TiO <sub>2</sub>	30% TiO <sub>2</sub>	% diff
ShowerLengthEnergyScale (mean, mm/eV)	0.5794	0.5748	0.79%
ShowerLengthEnergyScale (rms, mm/eV)	0.3589	0.3689	2.74%
MedianPlaneShowerWidth (mean)	1.389	1.381	0.577%
MedianPlaneShowerWidth (rms)	0.6778	0.6625	2.28%
GapScore2 (mean)	0.4806	0.4571	5.01%
GapScore2 (rms)	0.3682	0.3644	1.03%
GapScore1 (mean)	2.449	2.414	1.44%
GapScore1 (rms)	2.074	2.074	0%
Mass (mean, MeV/c <sup>2</sup> )	115.9	112.8	2.71%
Mass (rms, MeV/c <sup>2</sup> )	24.76	25.6	3.33%
Energy (mean, MeV)	692.5	673.3	2.81%
Energy (rms, MeV)	437.1	437.9	0.18%
EnergyRatio (mean)	0.7968	0.7918	0.62%
EnergyRatio (rms)	0.1278	0.116	9.68%
Number of blobs (mean)	1.478	1.476	0.13%
Number of blobs (rms)	0.5417	0.5377	0.74%

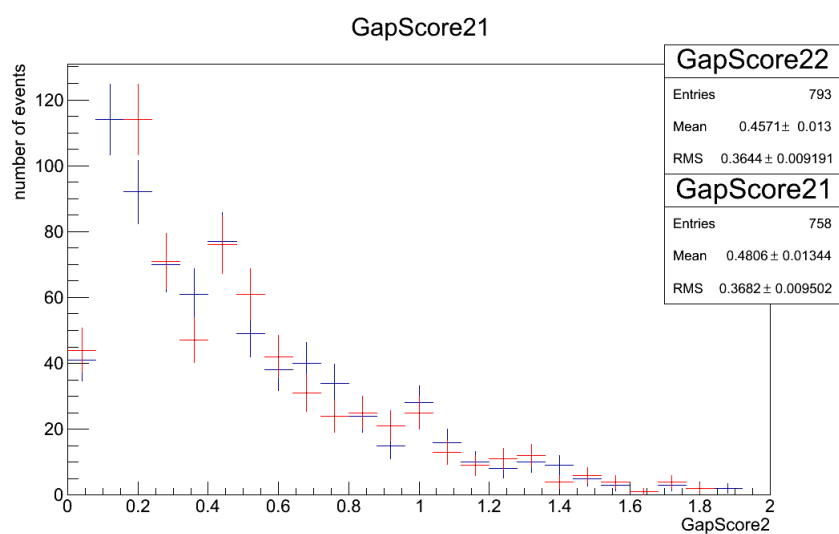


Figure 34: GapScore2, which indicates distance between low-peak-height clusters. The calculation of GapScore2 is described in sec. 2.2. GapScore21 depicts 15%  $\text{TiO}_2$ ; GapScore22 depicts a coating of 30%  $\text{TiO}_2$ .

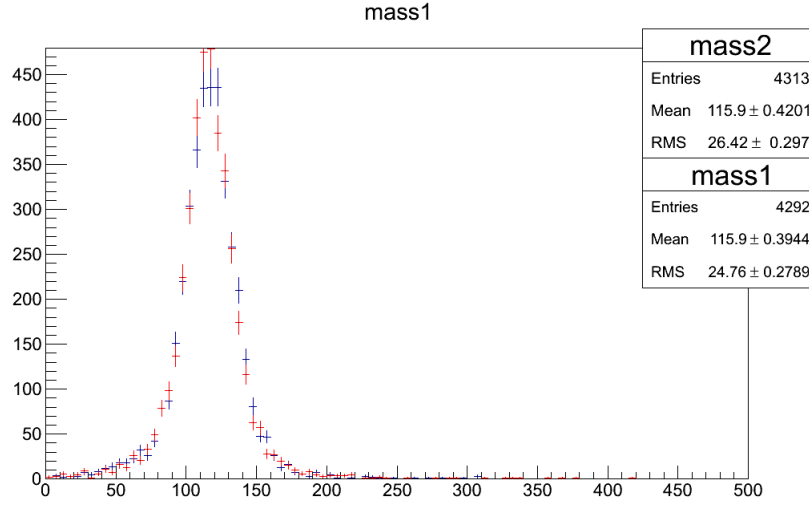


Figure 35: Reconstructed mass of  $\pi_0$  particles (in  $\text{MeV}/c^2$ ) vs. number of events. mass1 (blue) depicts 15%  $\text{TiO}_2$  bars by mass; mass2 (red) depicts 7.5%  $\text{TiO}_2$  by mass.

### 5.3 $\text{TiO}_2$ halved

It is also possible that the current detector reconstruction overestimates the amount of reflective coating on the scintillator bars. As before, it is extremely unlikely that the amount of titanium dioxide was overestimated by more than a factor of two; a 30%-40% error in amount of titanium used is much more likely. In this simulation, the scintillator bars were only 7.5%  $\text{TiO}_2$  by mass rather than 15% (in the original simulation).

We plotted the variables described in sec. 2.2 with 7.5 %  $\text{TiO}_2$  by mass in figs. 35 - 42, and summarize the mean and rms values in table 5.3.

We see a significant change in the RMS values of GapScore2 and reconstructed mass; however, neither mean changed more than 5%. In other words, halving the amount of  $\text{TiO}_2$  in the scintillator bars does not change the reconstruction of  $\pi_0$ s significantly, but doubling the amount of  $\text{TiO}_2$  does.

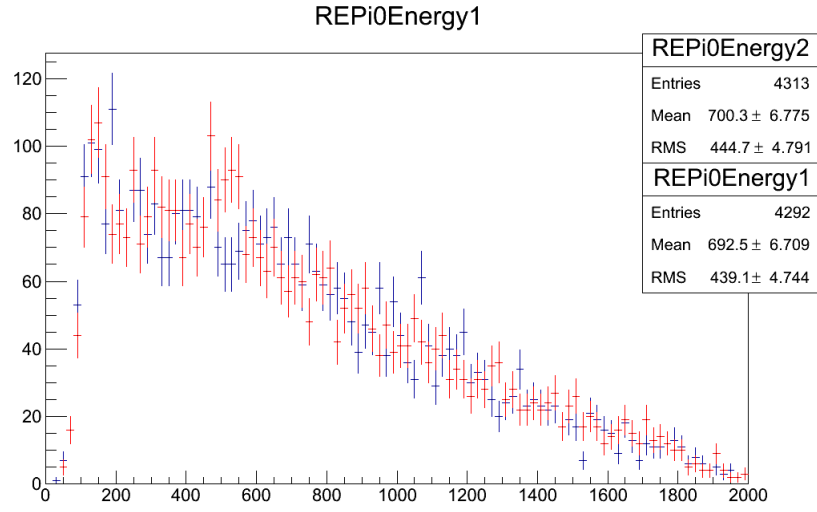


Figure 36: Reconstructed energy of  $\pi_0$  particles (in MeV) vs. number of events. energy1 (blue) depicts 15%  $\text{TiO}_2$  bars by mass; energy2 (red) depicts 7.5%  $\text{TiO}_2$  by mass.

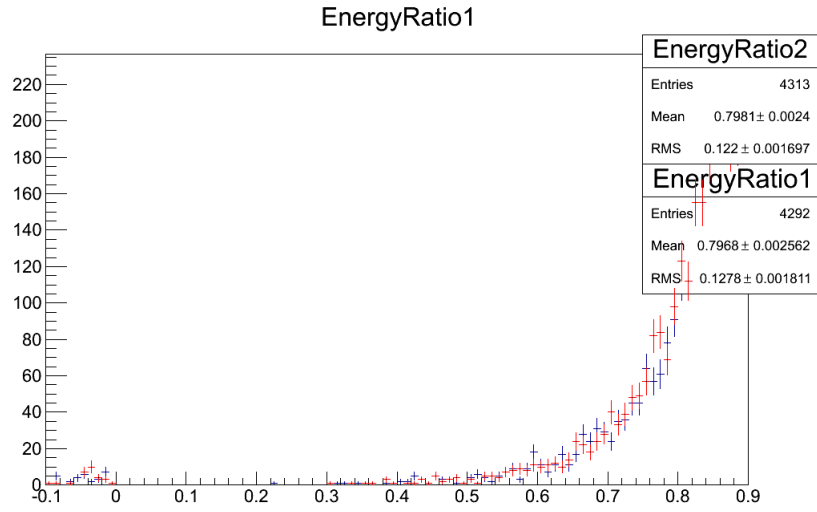


Figure 37: Ratio of reconstructed energy / Monte Carlo energy vs. number of events. EnergyRatio1 (blue) depicts 15%  $\text{TiO}_2$  bars by mass; EnergyRatio2 (red) depicts 7.5%  $\text{TiO}_2$  by mass.

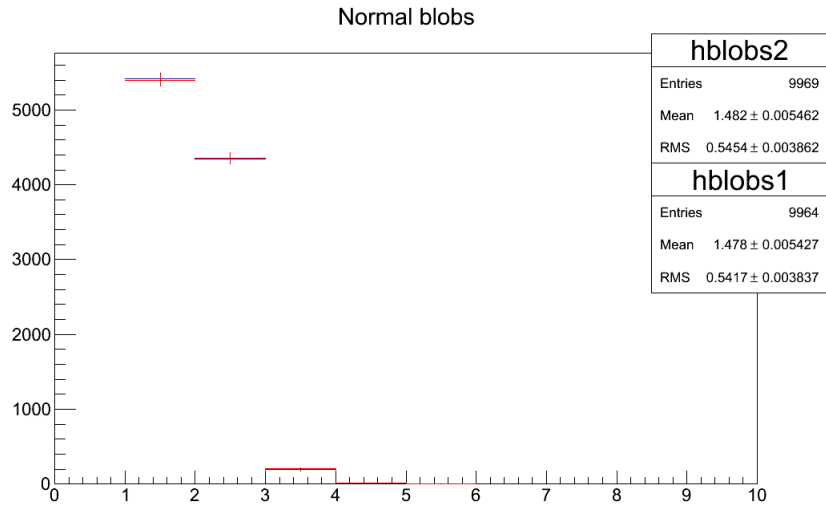


Figure 38: Number of AngleScan blobs vs. number of events. nblobs1 (blue) depicts 15%  $\text{TiO}_2$  bars by mass; nblobs2 (red) depicts 7.5%  $\text{TiO}_2$  by mass.

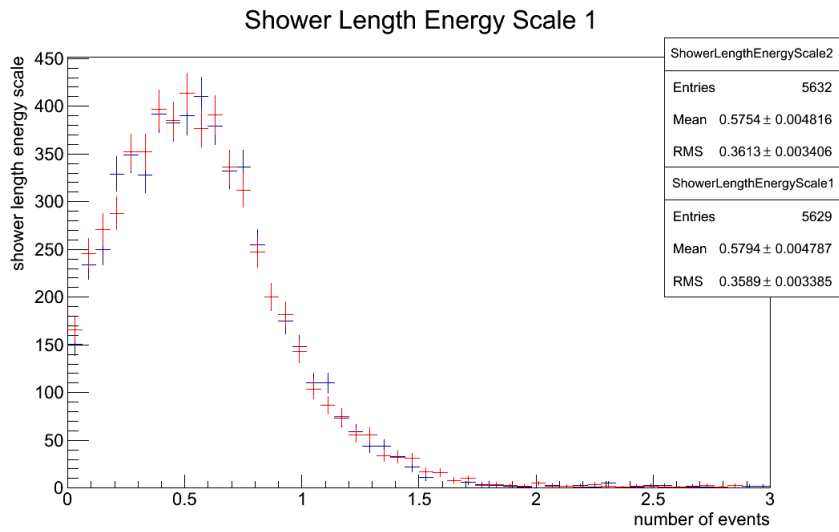


Figure 39: Shower length energy scale (mm/eV) or energy deposition profile. Algorithm described in section ?? . ShowerLengthEnergyScale1 (blue) depicts 15%  $\text{TiO}_2$  by mass; ShowerLengthEnergyScale2 (red) depicts 7.5%  $\text{TiO}_2$  by mass.

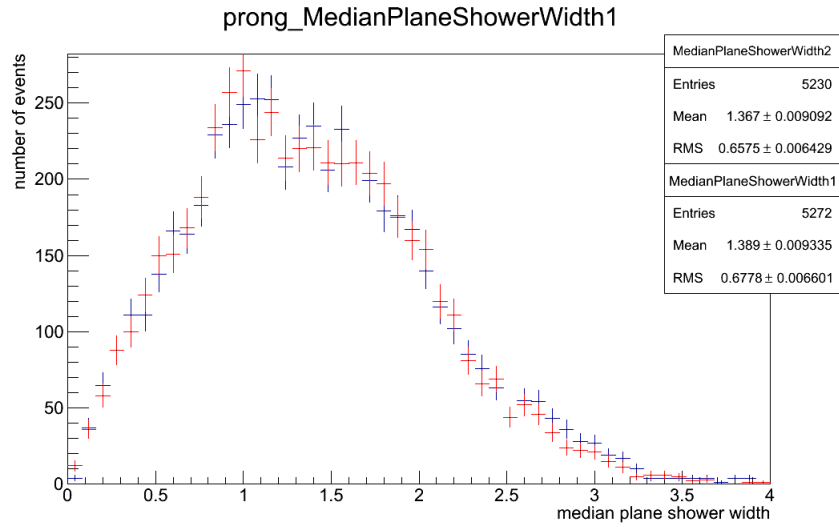


Figure 40: Median plane of deposition (strip number), which shows the shower width. Details of calculation are described in 2.2. MedianPlaneShowerWidth1 depicts 15%  $\text{TiO}_2$  by mass; MedianPlaneShowerWidth2 depicts 7.5%  $\text{TiO}_2$  by mass.

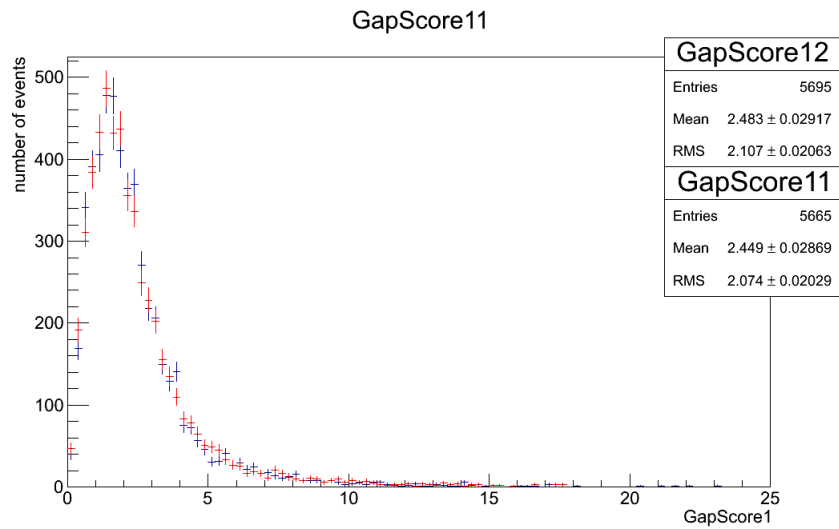


Figure 41: GapScore1, which indicates how spread apart the energy deposition of the shower was. The calculation of GapScore1 is described in sec. 2.2. GapScore11 depicts 15%  $\text{TiO}_2$ ; GapScore21 depicts a coating of 7.5%  $\text{TiO}_2$ .

Variable	15% TiO <sub>2</sub>	7.5% TiO <sub>2</sub>	% difference
ShowerLengthEnergyScale (mean, mm/eV)	0.5794	0.5754	0.69%
ShowerLengthEnergyScale (rms, mm/eV)	0.3589	0.3613	0.66%
MedianPlaneShowerWidth (mean)	1.389	1.367	1.59%
MedianPlaneShowerWidth (rms)	0.677	0.675	3.04%
GapScore2 (mean)	0.4806	0.4892	1.77%
GapScore2 (rms)	0.3682	0.4059	9.74%
GapScore1 (mean)	2.449	2.483	1.37%
GapScore1 (rms)	2.074	2.107	1.57%
Mass (mean, MeV/c <sup>2</sup> )	115.9	115.9	0%
Mass (rms, MeV/c <sup>2</sup> )	24.76	26.42	6.48%
Energy (mean, MeV)	692.5	700.3	1.12%
Energy (rms, MeV)	437.1	444.7	1.72%
EnergyRatio (mean)	0.7968	0.7981	0.16%
EnergyRatio (rms)	0.1278	0.122	4.68%
Number of blobs (mean)	1.478	1.482	0.27%
Number of blobs (rms)	0.5417	0.5454	0.68%



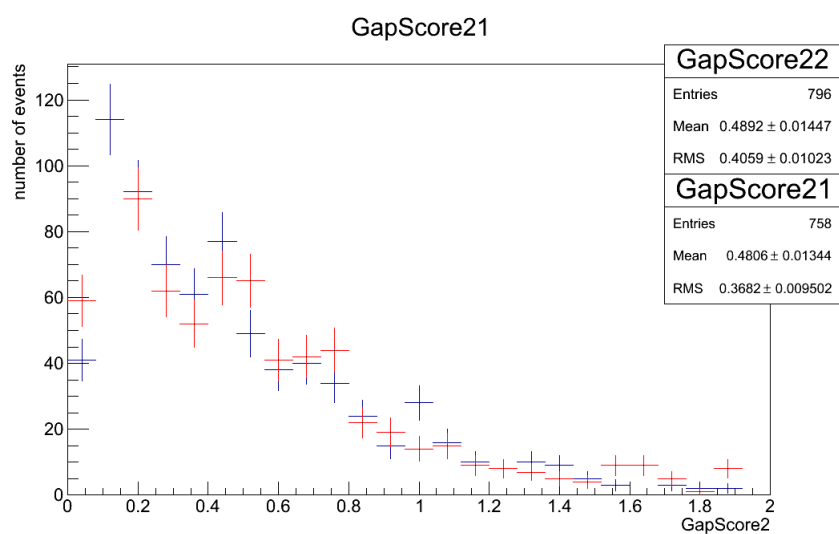


Figure 42: GapScore2, which indicates distance between low-peak-height clusters. The calculation of GapScore2 is described in sec. 2.2. GapScore21 depicts 15%  $\text{TiO}_2$ ; GapScore22 depicts a coating of 7.5%  $\text{TiO}_2$ .

## 5.4 Significance of results: halving, doubling, and reconstruction efficiency

This apparent contradiction is explained by considering the blobbing algorithm used in MCPi0/AngleScan. It looks for two blobs — no fewer, no less — and rejects the event if two blobs are not found.

The number of blobs decreases as the amount of  $\text{TiO}_2$  increases, as the characteristic interaction length in  $\text{TiO}_2$  is far shorter than the characteristic interaction length in scintillator. Therefore, events that might have three blobs with less  $\text{TiO}_2$  have two; events that might have two blobs with less  $\text{TiO}_2$  have one.

There are significantly fewer two-blob events accepted with doubled  $\text{TiO}_2$ . There are few events with three blobs (with the original  $\text{TiO}_2$  composition) that are shifted into the two-blob category with more  $\text{TiO}_2$ ; there are many events in the two-blob category (with original  $\text{TiO}_2$  composition) that are shifted to the one-blob category with more  $\text{TiO}_2$ . Therefore, in total, we see fewer two-blob (accepted) events, and the other variables change accordingly.

By contrast, there are many one-blob events with original composition; some of those are shifted to the two-blob category with less  $\text{TiO}_2$ . Fewer originally-one-blob events are counted as two blobs for low  $\text{TiO}_2$  than originally-two-blob events are counted as one-blob events with high  $\text{TiO}_2$ . There are very few three-blob events with the original composition, so the net accepted events should increase for low amounts of titanium dioxide, and decrease for high amounts of titanium dioxide.

It is also more difficult to read one-blob events as two-blob events than to read two-blob events as one-blob events. In the case of a one-blob event, there is often very little width to the shower; even with less material, nearly all of the energy is deposited in one place, and it is still classified as a one-blob event. By contrast, a two-blob event where the interactions occur close together can look like a one-blob event.

The shift in blob counted can be observed in the plots of number of blobs in an event — that is, fig. 30 (with 30%  $\text{TiO}_2$ ) and fig. 38 (with 7.5%  $\text{TiO}_2$ ). Correspondingly, we see more change in the variables that depend on blobbing (e.g. EnergyRatio) than in variables which do not use the AngleScan blobbing function (such as the CCNuE variables).

Lastly, and most importantly, the high  $\text{TiO}_2$  simulation adds more  $\text{TiO}_2$  (adding 15% by

mass so that the plastic scintillator region is 30% by mass  $\text{TiO}_2$ ) than the low  $\text{TiO}_2$  simulation subtracts (losing 7.5%  $\text{TiO}_2$  so the plastic scintillator region is 7.5%  $\text{TiO}_2$  by mass). Therefore, we expect to see more change in the doubled simulation than we do in the halved simulation. Indeed, we actually see only a few more accepted events for the halved  $\text{TiO}_2$  simulation (change of less than  $<20$  events). By contrast, we see  $\sim 2\%$  fewer accepted events for the doubled  $\text{TiO}_2$  simulation.

## 6 Conclusions

A factor of two change in mass fraction of titanium dioxide coating used in the detector simulation could shift RMS mass and RMS energy up to  $\sim 5\%$ . The blobbing algorithm used in AngleScan underestimates the  $\pi_0$  mass when there is more high Z material. This shift occurs only with reconstructions with a mass fraction of titanium dioxide coating than `MinervaMaterials.xml`. Since the amount of  $\text{TiO}_2$  used in detector construction was not precisely measured, it is possible but unlikely that this higher mass fraction of titanium dioxide (30% by mass) is a more accurate representation of the detector than our current simulation (15% by mass).

Similarly, a factor of two change in the mass fraction of kaolin in the “grey epoxy” creates a 2% shift in reconstructed mass. The amount of “grey epoxy” used during construction is better known than the amount of titanium dioxide used during construction. However, the density of kaolin in the detector simulation does not match the MSDS value — the epoxy does not use pure kaolin, but rather a kaolin-based mixture. The MSDS also suggests our mass fraction underestimates the fraction of kaolin actually used by 5% - 15%. The density and mass fraction used in the simulation should be changed to  $1.33 \text{ g/cm}^3$  and 20% kaolin, 80% resin respectively.